

Article

Short-to-Medium-Range Order and Atomic Packing in $Zr_{48}Cu_{36}Ag_8Al_8$ Bulk Metallic Glass

Yong Xu ^{1,*}, Meijie Yu ², Rongfu Xu ¹, Xianzhong Wang ¹, Zhigang Wang ¹, Yongfeng Liang ³ and Junpin Lin ^{3,*}

¹ School of Materials Science and Engineering, Shandong Jianzhu University, Jinan 250101, China; rongfu@sdjzu.edu.cn (R.X.); nu1961@163.com (X.W.); wzgsdu@126.com (Z.W.)

² School of Materials Science and Engineering, Shandong University, Jinan 250061, China; yumeijie@sdu.edu.cn

³ State Key Laboratory for Advanced Metals and Materials, University of Science and Technology Beijing, Beijing 100083, China; liangyf@skl.ustb.edu.cn

* Correspondence: xuyong2612@sdjzu.edu.cn (Y.X.); linjunpin@ustb.edu.cn (J.L.); Tel.: +86-531-8636-7286 (Y.X.)

Academic Editor: Jordi Sort Viñas

Received: 13 May 2016; Accepted: 19 September 2016; Published: 12 October 2016

Abstract: Due to its excellent glass-forming ability (GFA), the $Zr_{48}Cu_{36}Al_8Ag_8$ bulk metallic glass (BMG) is of great importance in glass transition investigations and new materials development. However, due to the lack of detailed structural information, the local structure and atomic packing of this alloy is still unknown. In this work, synchrotron measurement and reverse Monte Carlo simulation are performed on the atomic configuration of a Zr-based bulk metallic glass. The local structure is characterized in terms of bond pairs and Voronoi tessellation. It is found that there are mainly two types of bond pairs in the configuration, as the body-centered cubic (*bcc*)-type and icosahedral (*ico*)-type bond pairs. On the other hand, the main polyhedra in the configuration are icosahedra and the *bcc* structure. That is, the *bcc*-type bond pairs, together with the *ico*-type bond pairs, form the *bcc* polyhedra, introducing the distortion in *bcc* clusters in short range. However, in the medium range, the atoms formed linear or planar structures, other than the tridimensional clusters. That is, the medium-range order in glass is of 1D or 2D structure, suggesting the imperfect ordered packing feature.

Keywords: metallic glass; local structure; short range order; medium range order

PACS: 81.05.Kf

1. Introduction

$Zr_{48}Cu_{36}Al_8Ag_8$ bulk metallic glass (BMG) possesses an extraordinary glass-forming ability (GFA) of up to 20 mm in the smallest dimension, as well as large stability against crystallization in the supercooled liquid region [1–3]. This alloy provided the opportunity to investigate the nature of glass transition in BMGs and offered the possibility to develop a new generation of engineering materials [4]. However, the local structure and atomic packing, especially the short-range order (SRO) and medium-range order (MRO), of metallic glasses is still far from being understood due to the lack of detailed structural information [5]. Moreover, it is still unrevealed how the atomic structure affects the GFA in metallic alloys, despite several empirical rules having been proposed to evaluate the GFA [6,7]. The GFA of an alloy also depends on the kinetics of evolution and thermodynamically viable phases in its supercooled melt [8]. Therefore, it is crucial to predict BMGs with a large GFA by the understanding of the correlation of local structures and kinetics [9].

It is well known that icosahedral clusters exist in the BMG structure [10–13]. These icosahedral clusters with five-fold symmetry are incompatible with lattice periodicity, which will present a barrier for crystallization and improve the glassy formability [11]. However, the arrangement of the icosahedral clusters and the relationship between icosahedral clusters and other local structures are still not clear. The effects of the local structure in short and medium range on excellent GFA are also unknown. So far, however, few studies have been devoted to these important issues. In this paper, we present a reverse Monte Carlo [14] simulation of the atomic packing for the $Zr_{48}Cu_{36}Al_8Ag_8$ BMG. Bond pairs [15,16], bond-orientational order (BOO) parameters [17,18], and Voronoi tessellation [19,20] were used to characterize the SRO of the glassy state. Typical atomic clusters in short- and medium-range order were introduced and characterized from the three-dimensional (3D) realistic configuration.

2. Materials and Methods

Multicomponent alloy ingots with a nominal composition of $Zr_{48}Cu_{36}Al_8Ag_8$ were prepared by arc-melting under a high purity argon atmosphere. The ingots were re-melted five times to ensure chemical homogeneity and subsequently suction-cast into a copper mold (1-mm-thick plate). Pair distribution function (PDF) data of the samples annealed at 743 K were obtained from the in situ synchrotron X-ray diffraction measurements using the energy of 115 keV (corresponding to a X-ray wavelength of 0.10783 Å, which were carried out at the beamline 11-ID-C of the Advanced Photon Source, Argonne National Laboratory). Silicon crystal monochromator was employed to select the wavelength. High-resolution X-ray diffraction (HRXRD) patterns with large Q range were recorded on an image plate (MAR 345, with $100 \times 100 \mu\text{m}^2$ pixel size and a distance of 228.367 mm). Structural models for the liquids were obtained from Reverse Monte Carlo simulation (RMC) [14,21] simulations. The experimental $S(Q)$ and $G(r)$ data were modeled simultaneously by a new RMC code [22]. A randomly packed system with 4000 atoms was used as the initial configuration. An atomic guess configuration is generated by random atomic move and exchange, as well as density refinement by adjusting the box size. The number density calculated from the mass densities is 55.65 nm^{-3} . Following minimum interatomic distances (cutoffs) were applied: 0.269 nm for Zr-Zr, 0.240 nm for Zr-Cu, 0.254 nm for Zr-Ag, 0.253 nm for Zr-Al, 0.212 nm for Cu-Cu, 0.225 nm for Cu-Ag, 0.224 nm for Cu-Al, 0.239 nm for Ag-Ag, 0.238 nm for Ag-Al and 0.237 nm for Al-Al. In view of the effective application of potential constraints [23,24], the Morse potential was introduced in the RMC simulation.

Bond pair analysis is commonly adopted to describe the geometrical features of the atomic arrangement in a configuration [15,16]. It considers the bonding relations of an atomic pair, as well as the nearest neighbor atoms, in short range. Here, the bonding relation is not conferred as the chemical bonding, but the bonding determined by atomic distance, usually defined as cutoffs in simulation. There are four indexes for the description of local structure by the bond pairs, ($ijmn$). It is defined that: $i = 1$ represents the bonding of this atomic pair, while $i = 2$ represents the formless of this atomic pair; j represents the number of atoms bonding altogether with this atomic pair; m represents the number of bonds among these j atoms; n is a arbitrary number, defined to exclusively determine a bond pair. According to these definition, a fixed structure configuration can be described by several bond pair types. According to Honeycutt and Andersen's formula [15,16], 1551, 1541 and 1431 represent icosahedral (*ico*) bond pairs, 1441 and 1661 are body-centered cubic (*bcc*) bond pairs, 1421 is face-centered cubic (*fcc*) or hexagonal close-packed (*hcp*) bond pairs, and 1331, 1321, 1311 and 1211 are disordered atomic arrangements.

The bond-orientational order parameters were firstly proposed by Halperin and Nelson [25] for two-dimensional molten, as well as the description methods. It had been adopted by Steinhardt [17,18], Nelson [26] and Ronchetti (SNR) [18] to investigate the BOO of particles in a three-dimensional system. According to SNR, the line between two nearest neighbor coordination atoms are defined as a bond, whose orientation can be described by a selected spherical coordinates, as $\theta(r)$ and $\phi(r)$, neglecting the

length of the bond. Each bond are given a set of spherical harmonics, $Y_L^m[\theta(\mathbf{r}), \phi(\mathbf{r})]$, which is called the bond-orientational order parameters of this bond [17,18,26,27], as

$$Q_L^m(\mathbf{r}) = Y_L^m[\theta(\mathbf{r}), \phi(\mathbf{r})], \quad m = -L, \dots, 0, \dots, L \quad (1)$$

where \mathbf{r} represents the relative vector of bond center. Given two atoms with coordinates of $\mathbf{A}(x_1, y_1, z_1)$ and $\mathbf{B}(x_2, y_2, z_2)$, then $\mathbf{r}(x, y, z)$ is defined as (with spherical coordinates)

$$\phi(\mathbf{r}) = \arctan \frac{\sqrt{x^2 + y^2}}{z} \quad (2)$$

$$\theta(\mathbf{r}) = \arctan \frac{y}{x} \quad (3)$$

where $\mathbf{r} = (\mathbf{A} - \mathbf{B})/2$.

Given an atomic cluster, the commonly needed BOO is $\overline{Q_L^m}$, where $\overline{Q_L^m} = \langle Q_L^m \rangle$. The $\langle \cdot \rangle$ represents the average of BOO for all the nearest neighbor atoms. The value of $\overline{Q_L^m}$ depends on the selected coordinates. For the uniformity, the commonly used BOO is defined as the secondary rotation invariant parameters, as

$$Q_L = \left\{ \frac{4\pi}{2L+1} \sum_{m=-L}^L |\overline{Q_L^m}|^2 \right\}^{1/2} \quad (4)$$

where $|\overline{Q_L^m}|$ is a real number as the module of $\overline{Q_L^m}$, which sometime is a plurality.

The prominent feature of BOO is sensitive to the symmetry of the atomic clusters. Each atomic clusters has a relative set of Q_L , which can be adopted to describe the symmetry of clusters by calculating a few L values (with even number) [18]. Therefore, for a cluster formed by a center atom and N nearest neighbor atoms, a Q_{L-L} pattern will be composed by Q_L with different L values. According to Nelson [18,26], local BOO can be effectively described by the Q_{L-L} patterns. By calculating the several Q_L values, with the even L (except for zero), as $L = 0$, $Q_L = 1$ and $L = \text{odd number}$, $Q_L = 0$, the local BOO will be well described.

The configurations calculated by the simulations contain all the coordinates of the atoms, from which the all the Q_L values the clusters will be obtained, as well as the Q_{L-L} patterns. Then, the statistical distribution of BOO in the system can be derived and takes a comparison with the standard structures, restricted as the same coordination conditions.

For icosahedron clusters, the triple rotation invariant, \hat{W}_6 , of $Q_L^m(\mathbf{r})$ is very sensitive, which can be adopted to evaluate the orientational order of icosahedra. The formula of \hat{W}_6 is defined [28] as

$$\hat{W}_L = \frac{W_L}{\left[\sum_{m=-L}^L |\overline{Q_L^m}|^2 \right]^{3/2}} \quad (5)$$

where

$$W_L = \sum_{\substack{m_1, m_2, m_3 \\ m_1 + m_2 + m_3 = 0}} \begin{bmatrix} L & L & L \\ m_1 & m_2 & m_3 \end{bmatrix} \overline{Q_L^{m_1}} \overline{Q_L^{m_2}} \overline{Q_L^{m_3}} \quad (6)$$

where $\begin{bmatrix} L & L & L \\ m_1 & m_2 & m_3 \end{bmatrix}$ is the Wigner3j symbol, which can be calculated by the Racah formula

$$\begin{bmatrix} L_1 & L_2 & L_3 \\ m_1 & m_2 & m_3 \end{bmatrix} = (-1)^{L_1 - L_2 - m_3} \times \sqrt{\Delta(L_1 L_2 L_3)} \quad (7)$$

$$\sqrt{(L_1 - m_1)! (L_1 + m_1)! (L_2 - m_2)! (L_2 + m_2)! (L_3 - m_3)! (L_3 + m_3)!} \times \sum_t \frac{(-1)^t}{x}$$

where

$$x = t! (L_3 - L_2 + m_1 + t)! (L_3 - L_1 - m_2 + t)! (L_1 + L_2 - L_3 - t)! (L_1 - m_1 - t)! (L_2 + m_2 - t)! \quad (8)$$

$$\Delta(L_1 L_2 L_3) = \frac{(L_1 + L_2 - L_3)! (L_1 - L_2 + L_3)! (L_2 + L_3 - L_1)!}{(L_1 + L_2 + L_3 - 1)!}$$

The scale of t values, during the summation process, is calculated as

$$\max(0, L_2 - L_3 - m_1, L_1 - L_3 + m_2) \ll t \ll \min(L_1 + L_2 - L_3, L_1 - m_1, L_2 + m_2) \quad (9)$$

As being normalized, the values of \hat{W}_6 with arbitrary L are not affected by $Q_L^m(\mathbf{r})$ [18]. Table 1 illustrates the standard values of $|\hat{W}_L|$ for *ico*, *fcc*, *hcp* and *bcc* polyhedra. For ideal icosahedral symmetry, $|\hat{W}_L|$ is equal to 0.169754, while, for weak icosahedral symmetry, the value is very small.

Therefore, the distribution of $|\hat{W}_L|$ indicates the evolution of cluster symmetry. For an arbitrary atomic cluster, the structural type can be identified by comparing the $|\hat{W}_L|$ values of actual configuration and the standard crystalline [18].

It is known that the Voronoi polyhedrons in disordering systems have the same physical meaning with the Wigner-Seitz cells in ordering systems, which has been adopted to describe the atomic packing in SRO [29,30]. A Voronoi polyhedron around an atom can be defined as the minimum Kasper polyhedron with many planes. These planes are perpendicular to the basis vector between the center atom and the relative nearest neighbor atom. Voronoi analysis [19,31] adopts the Voronoi indexes $\langle n_3, n_4, n_5, n_6, \dots \rangle$ to describe the polyhedra. Here, n_i represents the number of the plane which has i edges, e.g., $i = 4$ represents the plane which is a quadrangle. Voronoi analysis can be used to identify the atomic packing characteristics. For examples, the *fcc* structures can be represented as $\langle 0, 12, 0, 0 \rangle$, indicating having 12 quadrangles only. The *bcc* structures can be represented by $\langle 0, 6, 0, 8 \rangle$, indicating having six quadrangles and eight hexagons. The *ico* structures can be represented by $\langle 0, 0, 12, 0 \rangle$, indicating having 12 pentagons. The summation of all the n_i numbers, as the sum of the Voronoi planes, indicates the coordination number (CN). That is, the CN of *fcc* is 12, *bcc* is 14, and *ico* is 12. Local volume of atoms, Ω_i , refers to the total volume of Voronoi polyhedron (including the volume of central atoms). It is worth to emphasize that the CN introduced by Voronoi polyhedron is actually the conjunction number [32], represented by Z , which has some difference with CN, e.g., $Z = 14$ for *bcc* but CN = 8.

Table 1. Standard W_L values for relative structures.

Alloys (Pearson)	Type	W_L				CN
		W_4	W_6	W_8	W_{10}	
Ni (<i>cF4</i>)	<i>fcc</i>	0.159317	0.013161	0.058455	0.090130	12
AlFe ₃ (<i>cF16</i>)	<i>fcc</i>	0.159318	0.013161	0.058455	0.090130	14
Ag (<i>hP2</i>)	<i>hcp</i>	0.134097	0.012431	0.050903	0.081962	12
Co ₃ Mo (<i>hP8</i>)	<i>hcp</i>	0.133902	0.012509	0.053965	0.001922	12
Fe (<i>cI2</i>)	<i>bcc</i>	0.159317	0.013161	0.058455	0.090130	8
CuZr (<i>cP2</i>)	<i>bcc</i>	0.159318	0.013161	0.058455	0.090130	14
Reference [18]	<i>ico</i>	undefined	0.169754	undefined	0.093967	13

3. Results

Figure 1 shows the experimental diffraction data and fitting spectra of the Zr₄₈Cu₃₆Al₈Ag₈ BMG, as well as the final 3 Dimensional atomic configuration after $\sim 10^7$ steps. Note that the calculated spectra are in good agreement with the experimental data for both the $S(Q)$ and $G(r)$ data. It should be pointed out that the potential energy of the modeled system descended from -2.22 eV of the initial configuration to -2.63 eV of the final configuration, implying that the final configuration is more energetically favorable with respect to other competition structures. All the above results imply that the final configuration is a favorable atomic structure for the Zr₄₈Cu₃₆Al₈Ag₈ BMG from both the

topological and energetic points of view. Through the fitting analysis for experimental spectra, the local structural parameters including CN and R were obtained.

Figure 2a shows the average CN distribution around each component. It is seen that the average CNs around Zr, Cu and Ag are mainly in the range of 13~15. However, the average CN around Al is mainly in the range of 11~13. This indicates that the local arrangements around Al atoms are different from other atoms. Figure 2b shows the BOO parameters of the RMC configuration. Here, we use the two BOO parameters, W_4 and W_6 , together to identify structures. For comparing the cubic and icosahedral symmetry, parameters (W_L) are provided. Because of symmetry, the first nonzero values of BOO parameters occur for $l = 4$ in clusters with cubic symmetry and for $l = 6$ in clusters with icosahedral symmetry [18]. As shown in Figure 2b, the values of the W_4 and W_6 parameters are nonzero, indicating the existence of cubic and icosahedral symmetry in SRO. However, the BOO parameters of the $Zr_{48}Cu_{36}Al_8Ag_8$ BMG are smaller than the relative standard cubic or icosahedral structures, indicating the extreme distortion of metallic glass clusters.

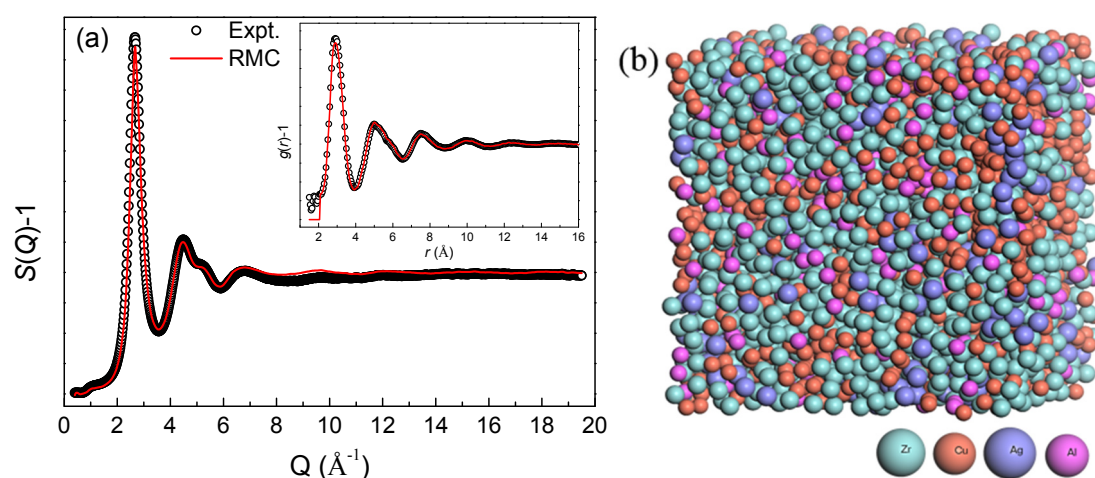


Figure 1. Reverse Monte Carlo modeling to reproduce the experimental synchrotron diffraction data. (a) The experimental structure factor (open circles), $S(Q)$, and fitting spectra (solid lines). PDF data is given as the inset pattern; (b) A review of the final RMC configuration.

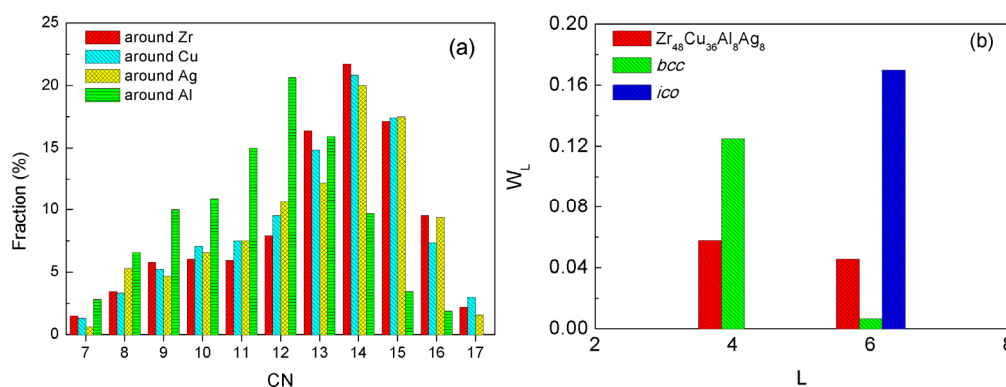


Figure 2. Distribution of (a) CN around Zr, Cu, Ag and Al atoms and (b) BOO parameters in $Zr_{48}Cu_{36}Al_8Ag_8$ BMG (red columns).

Figure 3a shows the distribution of bond pairs in the $Zr_{48}Cu_{36}Al_8Ag_8$ BMG. It is noted that the amount of *ico*-type bond pairs is remarkably greater than the *bcc*- and *fcc*-type (or *hcp*-type) bond pairs, as shown in Figure 3a. Therefore, it is evident that the *ico*-type bond pairs are dominant in

the $Zr_{48}Cu_{36}Al_8Ag_8$ glass structure, followed by the *bcc*-type bond pairs, indicating the presence of icosahedron short-range order (SRO) and the densely packed atomic structure.

As shown in Figure 3b, no dominant individual polyhedron with a frequency higher than 6% is formed. Of the polyhedra, the percentages of the Z13 $\langle 0, 3, 6, 4 \rangle$, Z14 $\langle 0, 2, 8, 4 \rangle$, Z14 $\langle 0, 3, 6, 5 \rangle$, Z14 $\langle 0, 4, 4, 6 \rangle$, Z14 $\langle 0, 4, 5, 5 \rangle$ and Z15 $\langle 0, 3, 6, 6 \rangle$ Kasper polyhedra are the highest, corresponding to the disordered *bcc*-type polyhedra with the three highest coordination numbers (CN = 13, 14 and 15). The total percentage of these polyhedra is $\sim 31.6\%$, as shown in Table 2. On the other hand, the total percentage of icosahedra Z12 $\langle 0, 0, 12, 0 \rangle$, together with distortion Z12 $\langle 0, 3, 6, 3 \rangle$, Z12 $\langle 0, 2, 8, 2 \rangle$ and Z13 $\langle 0, 1, 10, 2 \rangle$, is $\sim 7.2\%$, while a large number of other types take up small percentages.

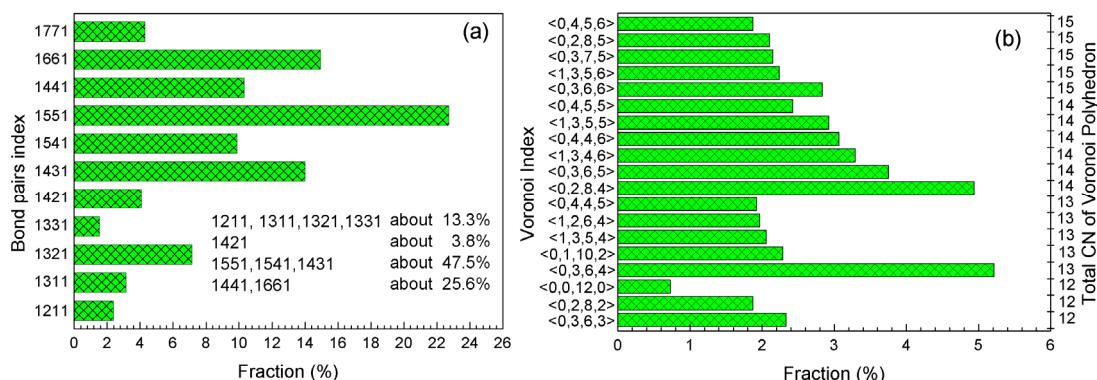


Figure 3. (a) Distribution of bond pairs in RMC configuration. The summation of some bond pairs is listed in the inset table down right; (b) Average frequencies of Voronoi polyhedra.

Table 2. The total percentage of *bcc*- and *ico*-type polyhedra in $Zr_{48}Cu_{36}Al_8Ag_8$ BMG.

Polyhedron Type	Fraction (%)				
	Total	Around Zr	Around Cu	Around Ag	Around Al
<i>bcc</i>	31.6	28.1	34.5	29.6	10.5
<i>ico</i>	7.2	5.8	7.5	6.5	29.0

Figure 4 shows some typical polyhedra in short-to-medium range obtained from the RMC configuration. The polyhedra with CN = 12 are typically of the icosahedral order, as shown in Figure 4a. On the other hand, the polyhedra with CN = 13 or 14 are of *bcc* order, as shown in Figure 4b,c. However, as calculated from BOO and Voronoi tessellation, the dominant atomic packing structures in the SRO are the distorted *bcc*- and *ico*-type clusters.

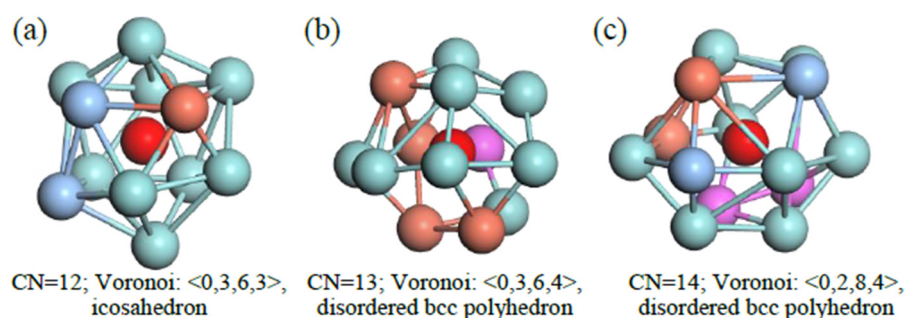


Figure 4. Cont.

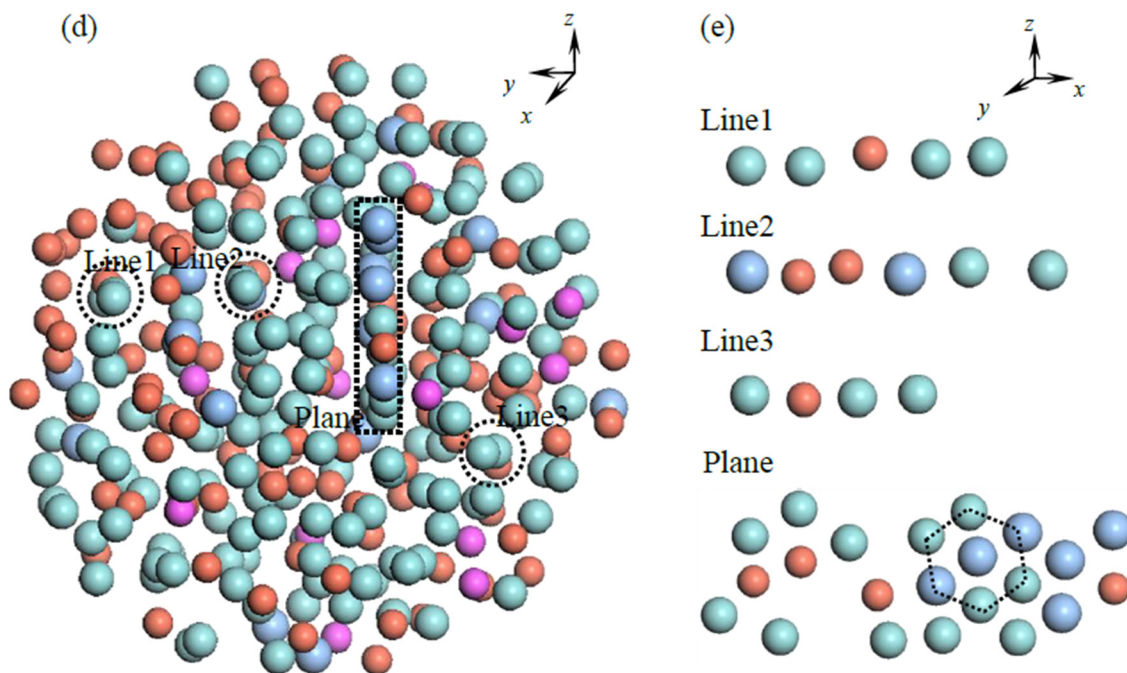


Figure 4. (a–c) Typical polyhedra in $Zr_{48}Cu_{36}Al_8Ag_8$ BMG. The Voronoi index and CN are also listed beneath the figures; (d) A randomly chosen cluster including four shells; (e) Atomic packing structures at medium range with a linear or planar packing type. The visual angle of the figure is defined by Cartesian coordinates, top right. The position of linear or planar packing atoms is marked by dashed circles or square in a four-shell cluster. However, the dashed hexagon marks the densely atomic packing region in the plane. In addition, the linear packing regions containing three atoms are not marked.

Figure 4d,e show a randomly selected cluster containing four coordinate shells, and the linear and planar packing atoms. The atoms distribute inhomogeneously in the whole space, and form some densely atomic packing regions, as marked by dashed circles and the square in Figure 4d. The linear-packed regions, as shown in Figure 4e, contain at least three to six atoms, which are densely packed in the medium range. The planar region contains a larger amount of atoms than the linear region. Most of the atoms in the planar region are densely packed, such as the region marked by the dashed hexagon in Figure 4e, even though free volumes exist. It can be seen that the planar region also contains lots of linear packing atoms.

4. Discussion

Clarifying the atomic packing characteristics of basic clusters will play a critical role in understanding the local structures of metallic glasses. The short-range order in metallic glasses should be apprehended by the coordinate polyhedra with two perspectives: the type of bond pairs and the coordinate shell [10]. It is believed that the structures of metallic glasses are described both in terms of the topology and the local distortion of the atomic bonds, among which the local distortion plays a dominant role [11]. To analyze the local structure and geometric feature of the atomic configuration, we employed the bond pair, BOO and Voronoi tessellation analysis techniques.

4.1. Short-Range Order of $ZrCuAlAg$

The local nearest-neighbor coordination can be determined unambiguously by using the Voronoi tessellation method to identify the possible clusters. The Voronoi index of each Voronoi polyhedron (coordinate polyhedron surrounding a central atom), $\langle n_3, n_4, n_5, n_6, \dots \rangle$, designates and differentiates the type of the coordinate polyhedron, where n_i denotes the number of i -edged faces of the Voronoi polyhedron and $\sum_i n_i$ is the total coordinate number (CN). The average CN of all atoms

is ~14.4 for the $Zr_{48}Cu_{36}Al_8Ag_8$ BMG, larger than that estimated from the first peak of the radial distribution function (RDF) profile (~13.3). In addition, such a CN would seem to also be larger than that determined by counting the number of atoms belonging to the 'first shell', which need to be predefined firstly by artificially selecting the cutoff distances. Thus, this procedure is very sensitive to the selected cutoff distances.

The existence of ISRO has been indirectly proved in the supercooled liquid and glass of unary and binary alloys by computational simulations [33]. It has also been assessed for Ni, Zr, and Ti from X-ray scattering and neutron-diffraction experiments combined with electromagnetic [34] and electrostatic [35] levitation techniques, and partially supported by ab initio molecular dynamics (AIMD) simulations [36]. It has been shown that an ISRO already exists in the stable liquid but local configurations are more complex than the simple icosahedron [37]. Moreover, this complexity has been found to depend on the system investigated and to increase in the supercooled region [36]. As studied before, the GFA is related to the presence of icosahedral order in Zr-Cu-Al ternary alloys [38]. Hui et al. [10] found that, comprehensively considering the topological and chemical SRO, Be makes a great contribution to the formation of icosahedral coordinate polyhedra, resulting in the improvement of the GFA for vit1(Zr41.2Ti13.8Cu12.5Ni10Be22.5) BMG alloy. As for the $Zr_{48}Cu_{36}Al_8Ag_8$ BMG, the addition of Ag in the Zr-Cu-Al alloy dramatically increases the glassy formability of the quaternary alloy [39].

It has been clarified that bond pairs in the $Zr_{48}Cu_{36}Al_8Ag_8$ BMG exhibit a strong tendency of icosahedral order, as shown in Figure 2a. Due to the relative high bonding energy, the number of icosahedral bond pairs is the highest among all kinds of bond pairs in the glassy state. The metallic systems have a tendency for dense packing to increase the number of atomic bonds to decrease the total energy. Therefore, except for forming the icosahedra, these icosahedral bond pairs, together with a small amount of *bcc*-type bond pairs, form the distorted *bcc* polyhedra. It can be seen that 1551, 1541 and 1431 pairs construct the icosahedra. Another part of the 1551, 1541 and 1431 pairs, together with 1661 and 1441 pairs, construct the disordered *bcc*-type polyhedra. Compared with the ordered *bcc* polyhedron in the crystalline structure, these distorted *bcc* polyhedra are preferred to form in short range, and they present a great barrier for building medium- and long-range lattice structures.

There are more than a hundred different types of coordination polyhedra formed in the RMC configuration, which have been previously reported and enumerated recently [40,41]. This finding suggests that the local arrangements cannot be modeled by a uniquely prescribed stereo-chemical unit [42]. On the other hand, some certain geometrically distinct polyhedra appear with high frequencies, as shown in Figure 3b. A comprehensive inspection [29] suggests that the underlying polyhedra in a number of MGs are Kasper polyhedra, which are the deltahedra that involve the minimal disclinations [27,43].

The average frequencies of Voronoi polyhedra around each component are also calculated, as shown in Table 2. There is no dominant individual polyhedron with a frequency higher than 6% formed. Of the polyhedra around Zr, Cu, and Ag, the total percentages of the disordered *bcc*-type polyhedra (CN = 13, 14, 15) have the highest total percentages, about 28.1%, 34.5%, and 29.6%, respectively. Meanwhile, the total percentages of icosahedra (CN = 11, 12, 13) are 5.8%, 7.5%, and 6.5%. This means that the distribution of *bcc*- and *ico*-type polyhedra around Zr, Cu, and Ag is similar. However, the total percentages of *bcc*- and *ico*-type polyhedra around Al are 10.5% and 29.0%, respectively. This indicates that, as for polyhedral clusters in the short range, disordered *bcc* polyhedra are the most favorable around Zr, Cu and Ag. However, the icosahedral order is more favorable than the *bcc*-type around Al. This suggests that Al plays a critical role in improving the icosahedral order in the $Zr_{48}Cu_{36}Al_8Ag_8$ BMG, which is consistent with the CN analysis.

The types of polyhedra and the distribution of CN are controlled by the atomic size ratio, R^* , between the solute and the solvent [42]. In binary systems, it has been found that, with decreasing R^* , the preferred polyhedron type changes from the Frank-Kasper type (for $R^* > 1.2$) to the icosahedral type ($R^* < 0.902$), then to the bi-capped square Archimedean anti-prism type ($R^* < 0.835$) and finally to

the tri-capped trigonal prism packing type ($R^* < 0.732$) [29]. In the $Zr_{48}Cu_{36}Al_8Ag_8$ BMG, however, for a solute atom, the solvent atoms involve all other components, resulting in a variety of R^* . As a result, more than three types of Voronoi polyhedra are formed with frequencies higher than 1%. This means that the structure of the $Zr_{48}Cu_{36}Al_8Ag_8$ alloy is highly distorted due to the formation of a variety of polyhedra.

It is believed that the *bcc* polyhedra in configuration is mainly generated and confined by experimental data (PDF). As for the $Zr_{48}Cu_{36}Al_8Ag_8$ BMG, the main type of the crystallized phase acts as a *bcc* structure. Thus, as the precursor of the *bcc* structure, the $Zr_{48}Cu_{36}Al_8Ag_8$ BMG also presents with the *bcc*-like characteristics, especially for SRO.

An icosahedron with 13 atoms is made of 20 tetrahedra and 42 atomic bonds, and is better packed than other polyhedral clusters [11], such as *fcc* and *bcc* polyhedra. In the $Zr_{48}Cu_{36}Al_8Ag_8$ BMG, a perfect icosahedron which entirely consists of 121,551 pairs with five-fold symmetry, and a distorted icosahedron which is mostly constituted of 1551 bond pairs together with an amount of 1541 or 1431 pairs, can be easily found. These icosahedra with five-fold symmetry introduce incompatibility with lattice periodicity development, and present a barrier for crystallization. On the other hand, according to the results of bond pair and Voronoi analyses, the dominant *bcc*-type polyhedra contain a lot of *ico*-type bond pairs, resulting in the distortion of the *bcc* polyhedron. The formation of *bcc*-type clusters is related to the structure of the high-temperature solid phase in the Zr-Cu alloy system. This means that the existence of distorted *bcc* polyhedra also prevents the formation of periodic structures.

4.2. Medium-Range Order and Atomic Packing Characteristics

To date, the medium-range order of metallic glasses is still an issue in the investigation of structure [44]. However, based on the RMC modeling, it is possible for us to get insight in the MRO, as the exact positions of all atoms in the glass structure are determined. After clarifying the clusters with several coordinate shells, the geometric and topological packing of MRO can be well described.

As shown in Figure 4d, all the atoms distribute inhomogeneously in a randomly selected cluster, forming some densely atomic packing regions. By changing the view angle of the 3D configuration of this cluster, the linear- and planar-packed regions are discovered, containing about three to 20 atoms. This means that the atoms tend to form the densely-packed linear and planar order regions in the medium range, as the medium-range order in the system. That is, unlike the SRO, the MRO in glasses is of one or two dimensions, suggesting the imperfect ordered packing feature [45,46].

For these densely-packed linear and planar order clusters, they must pack periodically along the normal direction of the atomic plane to construct the 3D crystalline structure. However, it is a diffusion process and it will consume extra energy for atoms to pack on the 3D scale. On the other hand, the symmetry of distorted *bcc* and *ico* polyhedra is incompatible with lattice periodicity, which also can prevent the formation of the crystalline structure in the 3D space. This indicates that the existence of the MRO also presents a barrier for crystallization in the $Zr_{48}Cu_{36}Al_8Ag_8$ BMG. As mentioned by Tanaka et al. [47], the dynamic heterogeneity was determined in several amorphous systems, which could also be described as the planar structures. It is found that this structural ordering has a direct connection to the dynamics of local configurational rearrangement, or structural relaxation. The finding of these linear and planar structures may bring some novel perspectives in the local structure of the BMG, which only assumes that the fully disordered configurations contain less MRO.

5. Conclusions

In summary, the atomic configuration of the $Zr_{48}Cu_{36}Al_8Ag_8$ BMG was simulated by means of the reverse Monte Carlo method. The analysis of bond pairs, BOO, and Voronoi polyhedra indicate that the extraordinary GFA of the $Zr_{48}Cu_{36}Al_8Ag_8$ BMG is essentially attributed to the following structural characteristics:

1. The densely packed disordered *bcc* and *ico* polyhedra are found dominantly in the SRO. The *bcc* polyhedra in configuration are mainly confined by the amorphous $Zr_{48}Cu_{36}Al_8Ag_8$ precursor, which has a *bcc*-like structure in the SRO.
2. The disordered *bcc* polyhedron contains a lot of *ico*-type bond pairs and prevents the formation of the periodic structures in the long range. The tendency of icosahedral ordering, as in the *ico*-type bond pairs and the icosahedra with five-fold symmetry, introduces the incompatibility with lattice periodicity in the system, presenting a barrier for crystallization.
3. The densely packed linear and planar ordering structures are found in the MRO, hindering the dynamic of local configuration rearrangement. It is suggested that this local structural feature stabilizes the supercooled liquid and prevents crystallization, resulting in the extraordinary GFA.

Acknowledgments: The authors would like to acknowledge the assistance of C. Fan. The authors also acknowledge the National Synchrotron Radiation Laboratory for assigning the beam-time. This work was supported by the National Natural Science Foundation of China (Grant No. 51101093) and Colleges and Universities in Shandong Province Science and Technology Plan Projects (J14LA04).

Author Contributions: Y.X. and J.P.L. conceived and designed the experiments; X.Z.W. performed the experiments; Z.G.W. and M.J.Y. analyzed the data; Y.F.L. and R.F.X. contributed reagents/materials/analysis tools; Y.X. wrote the paper.

Conflicts of Interest: The authors declare no conflict of interest.

References

1. Jiang, Q.K.; Wang, X.D.; Nie, X.P.; Zhang, G.Q.; Ma, H.; Fecht, H.J.; Bendnarcik, J.; Franz, H.; Liu, Y.G.; Cao, Q.P.; et al. Zr-(Cu,Ag)-Al bulk metallic glasses. *Acta Mater.* **2008**, *56*, 1785–1796. [[CrossRef](#)]
2. Zhang, Q.S.; Zhang, W.; Inoue, A. New Cu-Zr-based bulk metallic glasses with large diameters of up to 1.5 cm. *Scr. Mater.* **2006**, *55*, 711–713. [[CrossRef](#)]
3. Oh, J.C.; Ohkubo, T.; Kim, Y.C.; Fleury, E.; Hono, K. Phase separation in $Cu_{43}Zr_{43}Al_7Ag_7$ bulk metallic glass. *Scr. Mater.* **2005**, *53*, 165–169. [[CrossRef](#)]
4. Johnson, W. Bulk amorphous metal—An emerging engineering material. *JOM J. Miner. Met. Mater. Soc.* **2002**, *54*, 40–43. [[CrossRef](#)]
5. Cheng, Y.Q.; Ma, E.; Sheng, H.W. Atomic level structure in multicomponent bulk metallic glass. *Phys. Rev. Lett.* **2009**, *102*, 245501. [[CrossRef](#)] [[PubMed](#)]
6. Inoue, A. Stabilization of metallic supercooled liquid and bulk amorphous alloys. *Acta Mater.* **2000**, *48*, 279–306. [[CrossRef](#)]
7. Turnbull, D. Under what conditions can a glass be formed? *Contemp. Phys.* **1969**, *10*, 473–488. [[CrossRef](#)]
8. Li, Y.; Poon, S.J.; Shiflet, G.J.; Xu, J.; Kim, D.H.; Löffler, J.F. Formation of bulk metallic glasses and their composites. *MRS Bull.* **2007**, *32*, 624–628. [[CrossRef](#)]
9. Peng, H.L.; Li, M.Z.; Wang, W.H.; Wang, C.Z.; Ho, K.M. Effect of local structures and atomic packing on glass forming ability in Cu_xZr_{100-x} metallic glasses. *Appl. Phys. Lett.* **2010**, *96*, 021901–021903. [[CrossRef](#)]
10. Hui, X.; Fang, H.Z.; Chen, G.L.; Shang, S.L.; Wang, Y.; Qin, J.Y.; Liu, Z.K. Atomic structure of $Zr_{41.2}Ti_{13.8}Cu_{12.5}Ni_{10}Be_{22.5}$ bulk metallic glass alloy. *Acta Mater.* **2009**, *57*, 376–391. [[CrossRef](#)]
11. Egami, T. Icosahedral order in liquids. *J. Non-Cryst. Solids* **2007**, *353*, 3666–3670. [[CrossRef](#)]
12. Zhu, Z.W.; Zhang, H.F.; Sun, W.S.; Ding, B.Z.; Hu, Z.Q. Processing of bulk metallic glasses with high strength and large compressive plasticity in $Cu_{50}Zr_{50}$. *Scr. Mater.* **2006**, *54*, 1145–1149. [[CrossRef](#)]
13. Bernal, J.D. The bakerian lecture, 1962. The structure of liquids. *Proc. R. Soc. Lond. A* **1964**, *280*, 299–322. [[CrossRef](#)]
14. Keen, D.A.; McGreevy, R.L. Structural modelling of glasses using reverse monte carlo simulation. *Nature* **1990**, *344*, 423–425. [[CrossRef](#)]
15. Honeycutt, J.D.; Andersen, H.C. Molecular dynamics study of melting and freezing of small lennard-jones clusters. *J. Phys. Chem.* **1987**, *91*, 4950–4963. [[CrossRef](#)]
16. Shen, Y.T.; Kim, T.H.; Gangopadhyay, A.K.; Kelton, K.F. Icosahedral order, frustration, and the glass transition: Evidence from time-dependent nucleation and supercooled liquid structure studies. *Phys. Rev. Lett.* **2009**, *102*, 057801. [[CrossRef](#)] [[PubMed](#)]

17. Steinhardt, P.J.; Nelson, D.R.; Ronchetti, M. Icosahedral bond orientational order in supercooled liquids. *Phys. Rev. Lett.* **1981**, *47*, 1297–1300. [[CrossRef](#)]
18. Steinhardt, P.J.; Nelson, D.R.; Ronchetti, M. Bond-orientational order in liquids and glasses. *Phys. Rev. B* **1983**, *28*, 784–805. [[CrossRef](#)]
19. Finney, J.L. Random packings and the structure of simple liquids. I. The geometry of random close packing. *Proc. R. Soc. Lond. A* **1970**, *319*, 479–493. [[CrossRef](#)]
20. Finney, J.L. Random packings and the structure of simple liquids. II. The molecular geometry of simple liquids. *Proc. R. Soc. Lond. A* **1970**, *319*, 495–507. [[CrossRef](#)]
21. McGreevy, R.L. Reverse Monte Carlo modelling. *J. Phys. Condens. Matter* **2001**, *13*, R877–R913. [[CrossRef](#)]
22. Gereben, O.; Jovari, P.; Temleitner, L.; Pusztai, L. A new version of the RMC++ Reverse Monte Carlo programme, aimed at investigating the structure of covalent glasses. *J. Optoelectron. Adv. Mater.* **2007**, *9*, 3021–3027.
23. Kotbi, M.; Xu, H.; Habchi, M.; Dembahri, Z. Additional potential constraint in a reverse monte carlo (RMC) simulation. *Phys. Lett. A* **2003**, *315*, 463–466. [[CrossRef](#)]
24. Liu, X.J.; Chen, G.L.; Hui, X.; Liu, T.; Lu, Z.P. Ordered clusters and free volume in a Zr-Ni metallic glass. *Appl. Phys. Lett.* **2008**, *93*, 011911–011913. [[CrossRef](#)]
25. Halperin, B.I.; Nelson, D.R. Theory of two-dimensional melting. *Phys. Rev. Lett.* **1978**, *41*, 121–124. [[CrossRef](#)]
26. Nelson, D.R.; Toner, J. Bond-orientational order, dislocation loops, and melting of solids and smectic-A liquid crystals. *Phys. Rev. B* **1981**, *24*, 363–387. [[CrossRef](#)]
27. Nelson, D.R. Order, frustration, and defects in liquids and glasses. *Phys. Rev. B* **1983**, *28*, 5515–5535. [[CrossRef](#)]
28. Weisstein, E.W. Wigner 3j-Symbol. Available online: <http://mathworld.wolfram.com/Wigner3j-Symbol.html> (accessed on 22 September 2016).
29. Sheng, H.W.; Luo, W.K.; Alamgir, F.M.; Bai, J.M.; Ma, E. Atomic packing and short-to-medium-range order in metallic glasses. *Nature* **2006**, *439*, 419–425. [[CrossRef](#)] [[PubMed](#)]
30. Wang, X.D.; Yin, S.; Cao, Q.P.; Jiang, J.Z.; Franz, H.; Jin, Z.H. Atomic structure of binary Cu_{64.5}Zr_{35.5} bulk metallic glass. *Appl. Phys. Lett.* **2008**, *92*, 011902–011903. [[CrossRef](#)]
31. Finney, J.L. Modelling the structures of amorphous metals and alloys. *Nature* **1977**, *266*, 309–314. [[CrossRef](#)]
32. Zallen, R.; Huang, J. *Amorphous Solid State Physics*; Peking University Press: Beijing, China, 1988.
33. Jónsson, H.; Andersen, H.C. Icosahedral ordering in the lennard-jones liquid and glass. *Phys. Rev. Lett.* **1988**, *60*, 2295–2298. [[CrossRef](#)] [[PubMed](#)]
34. Schenk, T.; Holland-Moritz, D.; Simonet, V.; Bellissent, R.; Herlach, D.M. Icosahedral short-range order in deeply undercooled metallic melts. *Phys. Rev. Lett.* **2002**, *89*, 075507. [[CrossRef](#)] [[PubMed](#)]
35. Kelton, K.F.; Lee, G.W.; Gangopadhyay, A.K.; Hyers, R.W.; Rathz, T.J.; Rogers, J.R.; Robinson, M.B.; Robinson, D.S. First X-ray scattering studies on electrostatically levitated metallic liquids: Demonstrated influence of local icosahedral order on the nucleation barrier. *Phys. Rev. Lett.* **2003**, *90*, 195504. [[CrossRef](#)] [[PubMed](#)]
36. Jakse, N.; Pasturel, A. Local order of liquid and supercooled zirconium by ab initio molecular dynamics. *Phys. Rev. Lett.* **2003**, *91*, 195501. [[CrossRef](#)] [[PubMed](#)]
37. Jakse, N.; Pasturel, A. Local order and dynamic properties of liquid and undercooled Cu_xZr_{1-x} alloys by ab initio molecular dynamics. *Phys. Rev. B* **2008**, *78*, 214204–214209. [[CrossRef](#)]
38. Xu, Y.; Zhang, Y.; Tang, F.L.; Liu, X.J.; Chen, G.L. Effect of Al addition and icosahedral clusters on glass-forming ability and local structure of Zr_{50-x}Cu₅₀Al_x (x = 0–25) alloys. *J. Funct. Mater.* **2010**, *6*, 1042–1045.
39. Xu, Y.; Wang, Y.; Liu, X.; Chen, G.; Zhang, Y. Effects of additional elements (M) on the thermal stability and structure of (Zr_{52.2}Cu_{39.1}Al_{8.7})_{100-x}M_x (M = Ag, Be, Gd, x = 8, 7, 2) amorphous alloys. *J. Mater. Sci.* **2009**, *44*, 3861–3866. [[CrossRef](#)]
40. Borodin, V.A. Local atomic arrangements in polytetrahedral materials. *Philos. Mag. A* **1999**, *79*, 1887–1907. [[CrossRef](#)]
41. Borodin, V.A. Local atomic arrangements in polytetrahedral materials II. Coordination polyhedra with 14 and 15 atoms. *Philos. Mag. A* **2001**, *81*, 2427–2446. [[CrossRef](#)]
42. Luo, W.K.; Ma, E. EXAFS measurements and reverse Monte Carlo modeling of atomic structure in amorphous Ni₈₀P₂₀ alloys. *J. Non-Cryst. Solids* **2008**, *354*, 945–955. [[CrossRef](#)]

43. Doye, J.P.K.; Wales, D.J. The effect of the range of the potential on the structure and stability of simple liquids: From clusters to bulk, from sodium to C_{60} . *J. Phys. B At. Mol. Opt. Phys.* **1996**, *29*, 4859–4894. [[CrossRef](#)]
44. Hui, X.; Gao, R.; Chen, G.L.; Shang, S.L.; Wang, Y.; Liu, Z.K. Short-to-medium-range order in $Mg_{65}Cu_{25}Y_{10}$ metallic glass. *Phys. Lett. A* **2008**, *372*, 3078–3084. [[CrossRef](#)]
45. Chen, G.L.; Liu, X.J.; Hui, X.D.; Hou, H.Y.; Yao, K.F.; Liu, C.T.; Wadsworth, J. Molecular dynamic simulations and atomic structures of amorphous materials. *Appl. Phys. Lett.* **2006**, *88*, 203115. [[CrossRef](#)]
46. Liu, X.J.; Chen, G.L.; Hou, H.Y.; Hui, X.D.; Yao, K.F.; Lu, Z.P.; Liu, C.T. Atomistic mechanism for nanocrystallization of metallic glasses. *Acta Mater.* **2008**, *56*, 2760–2769. [[CrossRef](#)]
47. Tanaka, H.; Kawasaki, T.; Shintani, H.; Watanabe, K. Critical-like behaviour of glass-forming liquids. *Nat. Mater.* **2010**, *9*, 324–331. [[CrossRef](#)] [[PubMed](#)]



© 2016 by the authors; licensee MDPI, Basel, Switzerland. This article is an open access article distributed under the terms and conditions of the Creative Commons Attribution (CC-BY) license (<http://creativecommons.org/licenses/by/4.0/>).